Neutron Diffraction and FT-Raman Study of Ion-Exchangeable Layered Titanates and Niobates

Song-Ho Byeon* and Hyo-Jin Nam

College of Environment and Applied Chemistry, Kyung Hee University, Kyung Ki 449-701, Korea

Received October 18, 1999. Revised Manuscript Received March 9, 2000

On the basis of the structure refinements of neutron powder diffraction data, the Raman bands of $A_2La_2Ti_3O_{10}$ (A = Na, K, and Rb) were successfully assigned. The existence of a linear A−O−Ti linkage along the *c* axis in this structure resulted in the strong dependence of their Raman bands on the nature of the A atom. In contrast, the Raman spectra of $A_2La_2Ti_3O_{10}\cdot xH_2O$, $ACa_2Nb_3O_{10}$, and $ALaNb_2O_7$ (A = Na, K, Rb, and Cs) with no linear A−O−Ti or A−O−Nb connection were essentially the same in the 1000−400 cm^{-1} region regardless of a change of the A atom. In particular, the band around 930 cm^{-1} attributed to the terminal Nb−O bond with double-bond character showed no shift even in the Raman spectra of $CsB_2Nb_3O_{10}$ (B = Ca, Sr, and Ba) despite a remarkable change of lattice volume depending on the B atom. These results indicate that the Raman shift of ion-exchangeable perovskites depends mainly on the way that the interlayer alkali-metal atoms are connected with the octahedra in perovskite layers.

Introduction

One of the well-known layered oxides is composed of corner-shared BO_6 (B = Ti or Nb) octahedra which are periodically interleaved by the A cation layers of different structure.[1−4] Such oxides are generally formulated $A_m[A'_{n-1}B_nO_{3n+1}]$, where *m* corresponds to the interlayer charge and *n* represents the number of BO_6 octahedra in each layer. For instance, single- (*n* = 1) and triple- (*n* = 3) stacked TiO_6 octahedral slabs are units building blocks for $NaLn[TiO_4]$ and $A_2[Ln_2Ti_3O_{10}]$ (A = alkali-metal, Ln = lanthanides, *m* = 2), respectively, where the interlayer positions are occupied by the A atoms.[5,6] Similarly, $A[Ca_2Nb_3O_{10}]$ (*n* = 3, *m* = 1) and $A[LnNb_2O_7]$ (*n* = 2, *m* = 1) are built up of triple- and double-NbO_6 octahedral layers, respectively.[3,7]

Many investigations have been focused on the ion-exchange reaction of these materials in alkali-metal molten salts and aqueous acid solutions.[8−11] The proton-exchanged niobium oxides with a lower layer charge (*m* = 1) were used as host materials to intercalate a variety of organic bases and to polymerize the monomers inserted into their galleries.[7,12,13] In contrast, the protonated titanium oxides with a higher layer charge (*m* = 2) do not intercalate even strong organic bases. Furthermore, the intercalation behaviors of the niobium−titanium oxides showed a quite different intercalation behavior depending on the Nb/Ti ratios despite the same layer charge.[14] These results suggest that the interlayer chemistry of layered perovskites depends on the layer structure as well as the layer charge.

Recently, the photocatalytic activities of these layered perovskites were investigated. Under visible light irradiation, $RbPb_2Nb_3O_{10}$- (*m* = 1, *n* = 3 member) based catalysts were found to evolve H_2 from an aqueous methanol solution.[15] $A_{2-x}La_2Ti_{3-x}Nb_xO_{10}$ (solid solution between *m* = 1, *n* = 3 and *m* = 2, *n* = 3 members) also showed high activity for the photocatalytic decomposition of water.[16,17] The remarkable shape selectivity and dependence of the catalytic activity on the hydration suggested an important role of the interlayer space. However, a tentative mechanism proposed for this photocatalytic reaction was not based on a deep understanding of the interlayer space.

The crystal structures of many *m* = 1 and 2 members were determined by X-ray and neutron diffraction.[4,18−21]

* To whom correspondence should be addressed.

(1) Ruddlesden, S. N.; Popper, P. *Acta Crystallogr.* **1957**, *10*, 538.
(2) Tilley, R. J. D. *J. Solid State Chem.* **1977**, *21*, 293.
(3) Dion, M.; Ganne, M.; Tournoux, M. *Mater. Res. Bull.* **1981**, *16*, 1429.
(4) Dion, M.; Ganne, M.; Tournoux, M.; Ravez, J. *Rev. Chim. Miner.* **1984**, *21*, 92.
(5) Gopalakrishnan, J.; Bhat, V. *Inorg. Chem.* **1987**, *26*, 4301.
(6) Blasse, G. *J. Inorg. Nucl. Chem.* **1968**, *30*, 656.
(7) Gopalakrishnan, J.; Bhat, V.; Raveau, B. *Mater. Res. Bull.* **1987**, *22*, 413.
(8) Jacobson, A. J.; Lewandowski, J. T.; Johnson, J. W. *J. Less-Common Met.* **1986**, *116*, 137.
(9) Subramanian, M. A.; Gopalakrishnan, J.; Sleigth, A. W. *Mater. Res. Bull.* **1988**, *23*, 837.
(10) Sato, M.; Watanabe, J.; Uematsu, K. *J. Solid State Chem.* **1993**, *107*, 460.
(11) Byeon, S.-H.; Yoon, J.-J.; Lee, S.-O. *J. Solid State Chem.* **1996**, *127*, 119.
(12) Jacobson, A. J.; Johnson, J. W.; Lewandowski, J. T. *Mater. Res. Bull.* **1987**, *22*, 45.
(13) Uma, S.; Gopalakrishnan, J. *Mater. Sci. Eng. B* **1995**, *34*, 175.
(14) Gopalakrishnan, J.; Uma, S.; Bhat, V. *Chem. Mater.* **1993**, *5*, 132.
(15) Yoshimura, J.; Ebina, Y.; Kondo, J.; Domen, K.; Tanaka, A. *J. Phys. Chem.* **1993**, *97*, 1970.
(16) Takata, T.; Furumi, Y.; Shinohara, K.; Tanaka, A.; Hara, M.; Kondo, J.; Domen, K. *Chem. Mater.* **1997**, *9*, 1063.
(17) Ikeda, S.; Hara, M.; Kondo, J.; Domen, K.; Takahashi, H.; Okubo, T.; Kakihana, M. *Chem. Mater.* **1998**, *10*, 72.
(18) Armstrong, A. R.; Anderson, P. A. *Inorg. Chem.* **1994**, *33*, 4366.
(19) Toda, K.; Kameo, Y.; Fujimoto, M.; Sato, M. *J. Ceram. Soc. Jpn.* **1993**, *101*, 980.
(20) Richard, M.; Brohan, L.; Tournoux, M. *J. Solid State Chem.* **1994**, *112*, 345.

10.1021/cm9906506 CCC: $19.00
Published on Web 05/16/2000

Nevertheless, the correlation between the structure of interlayer space and the interlayer chemistry such as ion-exchange reaction, intercalation reaction, and catalytic reaction is not well understood. This may be due to the poor crystallinity of the host/guest composites during or after interlayer reactions. In this case, Raman spectroscopy would be effective to investigate a change of local structure. We have previously reported the Raman spectra of layered titanium oxides, $NaLnTiO_4$ and $Na_2Ln_2Ti_3O_{10}$ (Ln = lanthanides).[22] Such a study clearly demonstrated that a change of interlayer structure results in a considerable shift of the characteristic Raman bands closely related to the sodium layer. In the present work, the Raman spectra of ion-exchangeable titanium and niobium oxides were investigated to correlate the Raman shifts with a difference in the structure of interlayer and multiple-octahedral slab. $A_2La_2Ti_3O_{10}$ (A = Na, K, and Rb) and their hydrated forms were selected as reference compounds for m = 2 members. Comparison of the Raman spectra for $ALaNb_2O_7$ and $ACa_2Nb_3O_{10}$ (A = Na, K, Rb, and Cs) with different thickness of the octahedral slab led to a reasonable assignment of the characteristic Raman bands for m = 1 members. The Raman shifts affected by the expansion of perovskite slab were analyzed using $CsB_2Nb_3O_{10}$ (B = Ca, Sr, and Ba). Understanding the interlayer structure−Raman spectra relationship shown in this report would be essential to elucidate a chemical reaction in the interlayer space.

Experimental Section

Synthesis. $A_2La_2Ti_3O_{10}$ (A = Na, K, Rb), $ACa_2Nb_3O_{10}$ and $ALaNb_2O_7$ (A = K, Rb, Cs), and $CsB_2Nb_3O_{10}$ (B = Ca, Sr, and Ba) were prepared by heating an appropriate mixture of A_2CO_3, La_2O_3, BCO_3, Nb_2O_5, and TiO_2 in air at 1000−1150 °C for 2 days with two intermittent grindings.[3−7] An excess (~20 mol %) of A_2CO_3 was added to compensate for the loss of volatile alkali-metal components. After the reaction, the products were washed with distilled water and dried at 120 °C. The hydrated forms of $A_2La_2Ti_3O_{10}$ were obtained when the samples were dried at room temperature after the washing rather than at 120 °C. $NaLaNb_2O_7$ and $NaCa_2Nb_3O_{10}$ were prepared by the ion-exchange reaction; 1 g of parent oxide such as $KLaNb_2O_7$ and $KCa_2Nb_3O_{10}$ was treated with 10 g of molten $NaNO_3$ at 300 °C for 2 days. $NaNO_3$ was replaced once in between. The product was washed with hot water and dried at 120 °C.

Analysis. A stoichiometric composition was confirmed by the elemental analysis of alkali metal using the inductively coupled plasma (ICP) and the energy-dispersive X-ray emission (EDX) techniques. The temperature higher than 600 °C was required for a complete dehydration of $A_2La_2Ti_3O_{10}{\cdot}xH_2O$ and the amount (x) of intercalated water was estimated by heating (2 °C/min) the samples in air to 800 °C. A weight loss from 100 °C up to ~700 °C corresponded to ~2 H_2O per formula unit.

X-ray Diffraction. The powder X-ray diffraction patterns were recorded on a rotating anode installed diffractometer (18 kW). The Cu Kα radiation used was monochromated by a curved-crystal graphite. All the patterns for oxides prepared in this work were indexed on the basis of tetragonal or orthorhombic cell and in well agreement with the literature data.[3,5,7,14,23] Data for structure refinement of $A_2La_2Ti_3O_{10}$ (A = K and Rb) were collected with a step-scan procedure in the range $2\theta = 10-110°$ with a step width of 0.02° and a step time of 1s. The structural refinements of their patterns were carried out using the Rietveld analysis programs RIETAN.[24]

Neutron Diffraction. Neutron powder diffraction measurements were performed on the high-resolution powder diffractometer (HRPD) at the HANARO center of the Korea Atomic Energy Research Institute (KAERI). The structural refinements were achieved using the Rietveld analysis programs RIETAN and FULLPROF.[25]

Raman Spectroscopy. Raman spectra were obtained with a Bruker RFS 100/S FT-Raman spectrometer coupled to the high sensitivity Raman detector (model D 418-S), which was cooled to liquid nitrogen temperature. Powdered samples packed into small aluminum cups were excited by the 1064 nm line of the Nd:YAG laser with 10 mW of power. The laser beam was focused on the sample, and the scattered light was collimated into the spectrometer by 180° angle configuration. Raman spectra were collected at room temperature. In-situ Raman study for the dehydration of $A_2La_2Ti_3O_{10}{\cdot}xH_2O$ ($x \approx 2$) oxides above room temperature were performed using a variable-temperature cell provided by Bruker. The cell was capable of operating up to 200 °C. The overall spectral resolution of the spectra was determined to be about 2 cm^{-1}.

Results and Discussion

Structure Refinement of $A_2La_2Ti_3O_{10}$ (A = K and Rb). The reliable structure data should be required for a reasonable interpretation of the Raman spectra. Since no structural information for $A_2La_2Ti_3O_{10}$ except A = Na analogue could be obtained from the literature, the X-ray diffraction patterns for A = K and Rb were analyzed by the Rietveld method. On the basis of the extinction condition, $h + k + l = 2n$ for hkl reflection, the crystal structure of these compounds was refined using initial atomic positions of $Na_2La_2Ti_3O_{10}$ with space group $I4/mmm$.[19] Corrections for a (00l) preferred orientation were made for all phases in the final stage of the refinement. Some crystallographic data and the refined atomic parameters are compared with those of $Na_2La_2Ti_3O_{10}$ in Table 1. Although the agreeable reliability factors are obtained, the four equivalent O(1)'s have an exceptionally high isotropic temperature parameter (B = 4−8 Å^2) for all compounds. Through a reexamination using time-of-flight powder neutron diffraction, Wright et al.[26] proposed that an acceptable temperature factor for those oxygens of $Na_2La_2Ti_3O_{10}$ is obtained only by shifting their positions from ideal 4c (0, 0.5, 0) to half-occupied sites 8j (x, 0.5, 0). The axial O(2) and O(4), and the Na and La sites were also allowed to move off the ⟨001⟩ axis to 16n (x, 0, z) sites. The refinement with such shifted atomic positions showed that the corner-shared $Ti(1)O_6$ octahedra are relatively rotated and tilted about the c axis.

To compare the structural changes on the same condition, the structure refinement was carried out again for the neutron powder diffraction data of $K_2La_2Ti_3O_{10}$ and $Rb_2La_2Ti_3O_{10}$ according to Wright et al. Some crystallographic data and final reliability factors are listed in Table 2. The observed, calculated, and difference profile for $K_2La_2Ti_3O_{10}$ is shown in Figure 1.

(21) Byeon, S.-H.; Park, K.; Itoh, M. *J. Solid State Chem.* **1996**, *121*, 430.
(22) Byeon, S.-H.; Lee, S. O.; Kim, H. *J. Solid State Chem.* **1997**, *130*, 110.
(23) Uma, S.; Raju, A. R.; Gopalakrishnan, J. *J. Mater. Chem.* **1993**, *3*, 709.
(24) Izumi, F.; Murata, H.; Watanabe, N. *J. Appl. Crystallogr.* **1987**, *20*, 411.
(25) Rodriguez-Carvajal, J. *Full Prof.98*; Laboratoire Leon Brillouin, 1998.
(26) Wright, A. J.; Greaves, C. *J. Mater. Chem.* **1996**, *6*, 1823.

Table 1. X-ray Diffraction Data for Atomic Positions and Isotropic Temperature Factors of $A_2La_2Ti_3O_{10}$ (A = Na, K, and Rb)

compound	atom	position	g^a	x	y	z	B (Å^2)
$Na_2La_2Ti_3O_{10}$[b]	La	4e	4	0.0	0.0	0.4246(1)	0.06(11)
	Na	4e	4	0.0	0.0	0.2895(9)	0.5
	Ti(1)	2a	2	0.0	0.0	0.0	0.1
	Ti(2)	4e	4	0.0	0.0	0.1491(4)	0.1
	O(1)	4c	4	0.0	0.5	0.0	8(2)
	O(2)	4e	4	0.0	0.0	0.065(1)	0.5
	O(3)	8g	8	0.0	0.5	0.137(1)	0.4(6)
	O(4)	4e	4	0.0	0.0	0.210(1)	0.8(8)
$K_2La_2Ti_3O_{10}$[c]	La	4e	4	0.0	0.0	0.42775(3)	0.71(2)
	K	4e	4	0.0	0.0	0.29193(8)	0.87(9)
	Ti(1)	2a	2	0.0	0.0	0.0	0.48(9)
	Ti(2)	4e	4	0.0	0.0	0.14155(8)	0.20(6)
	O(1)	4c	4	0.0	0.5	0.0	5.9(4)
	O(2)	4e	4	0.0	0.0	0.0622(3)	1.1(2)
	O(3)	8g	8	0.0	0.5	0.1285(2)	0.6(1)
	O(4)	4e	4	0.0	0.0	0.2001(2)	0.4(2)
$Rb_2La_2Ti_3O_{10}$[d]	La	4e	4	0.0	0.0	0.42960(6)	0.45(4)
	Rb	4e	4	0.0	0.0	0.29248(8)	1.30(7)
	Ti(1)	2a	2	0.0	0.0	0.0	0.68(7)
	Ti(2)	4e	4	0.0	0.0	0.1373(1)	0.32(6)
	O(1)	4c	4	0.0	0.5	0.0	4.2(5)
	O(2)	4e	4	0.0	0.0	0.0637(6)	1.3(3)
	O(3)	8g	8	0.0	0.5	0.1237(3)	0.9(2)
	O(4)	4e	4	0.0	0.0	0.1929(4)	0.6(2)

[a] Unit cell occupancy. [b] Toda et al. (ref 19). [c] $K_2La_2Ti_3O_{10}$: a = 3.8697(6) Å, c = 29.775(5) Å, R_I = 3.57%, R_{WP} = 10.91%, R_E = 4.60%. [d] $Rb_2La_2Ti_3O_{10}$: a = 3.89538(4) Å, c = 30.4650(4) Å, R_I = 2.96%, R_{WP} = 13.69%, R_E = 7.57%.

Table 2. Neutron Powder Diffraction Data of $A_2La_2Ti_3O_{10}$ Where A = Na, K, and Rb

	$Na_2La_2Ti_3O_{10}$[a]	$K_2La_2Ti_3O_{10}$	$Rb_2La_2Ti_3O_{10}$
space group	*I*4/*mmm*	*I*4/*mmm*	*I*4/*mmm*
a (Å)	3.84397(3)	3.89318(9)	3.91803(9)
c (Å)	28.5882(4)	29.9557(9)	30.6608(9)
Z	2	2	2
V (cm^3)	422.42	454.03(3)	470.67(4)
Bragg (R_I, %)		4.04	6.26
weighted profile (R_{WP}, %)	5.67	7.32	6.37
profile (R_P, %)	5.40	5.29	4.74
expected (R_E, %)	1.90	4.14	4.09

[a] Wright et al. (ref 26).

Refined atomic positions and isotropic temperature factors are compared with those of $Na_2La_2Ti_3O_{10}$ in Table 3. When we compare with Table 1, the temperature factors of O(1) were largely reduced for both $K_2La_2Ti_3O_{10}$ and $Rb_2La_2Ti_3O_{10}$ as expected. Selected bond lengths and bond angles of $A_2La_2Ti_3O_{10}$ (A = Na, K, and Rb) are summarized in Table 4. The ideal structure illustrated in Figure 2 is composed of highly distorted outer Ti(2)O_6 octahedral layers, which are induced by a displacement of Ti(2) atom from the center of its octahedron toward the alkali-metal layers, and weakly distorted central Ti(1)O_6 ones. The A atoms occupy all of 9-coordinate sites in the interlayer space and the A−O(4)−Ti(2) linkage is essentially linear.

As shown in Table 3, the deviation of O(1) from ideal position 4c (0, 0.5, 0) gives a rotation of Ti(1)O_6 octahedra about the c axis. Such a structural feature is true for all of A = Na, K, and Rb analogues. No noticeable difference in rotation angles is observed (∼12.5°). Comparing the Ti(1)−O(2)−Ti(2) bond angle of three compounds, the tilting degree of the octahedra is also constant within experimental errors. A gradual increase of the Ti(1)−O(1) bond length when the A atom changes from Na to Rb is in agreement with a lattice expansion. In contrast to such a general behavior, it would be quite unusual that an unexpected change in length is observed with the Ti(1)−O(2) bond; its length decreases from $Na_2La_2Ti_3O_{10}$ (1.924 Å) to $K_2La_2Ti_3O_{10}$ (1.918 Å) and $Rb_2La_2Ti_3O_{10}$ (1.900 Å) despite the expansion along the c axis. Shortening of the axial Ti(1)−O(2) bond and lengthening of the equatorial Ti(1)−O(1) bond must induce an increased compression of Ti(1)O_6 octahedra. The degree of distortion could be represented by the bond length ratio ($\theta = d\{\text{Ti(1)−O(2)}\}/d\{\text{Ti(1)−O(1)}\}$) which decreases from 0.977 (A = Na) to 0.961 (A = K) and 0.949 (A = Rb).

The strong distortion of Ti(2)O_6 octahedra gives rise to a quite short Ti(2)−O(4) and a long Ti(2)−O(2) bonds and a considerable bending of O(3)−Ti(2)−O(3) bonds for the A = Na analogue. On replacing Na by K and Rb, a significant increase in length is observed for the Ti(2)−O(4) bond. This indicates that the nature of A atom strongly influences on the competing Ti−O bond because the A−O−Ti linkage is practically linear in this structure. On the other hand, the Ti(2)−O(2) bond length decreases from A = Na to K and Rb. Such a shortening is also accompanied by an increase of O(3)−Ti(2)−O(3) bond angle. This, coupled with a decreased difference (Δ) in length between the Ti(2)−O(2) and Ti(2)−O(4) bonds (Δ = 0.656 Å, 0.548 Å, and 0.497 Å for A = Na, K, and Rb, respectively), indicates that the distortion of Ti(2)O_6 octahedra is reduced in this sequence. Interestingly, the distortion behaviors of Ti(1)O_6 and Ti(2)O_6 octahedra were reflected quite well in their Raman spectra when the interlayer atom was changed.

Raman Spectra of $A_2La_2Ti_3O_{10}$ (A = Na, K, and Rb) and Their Hydrates. In our previous study on the Raman spectra of $Na_2Ln_2Ti_3O_{10}$ (Ln = lanthanides),[22] the characteristic Raman bands were visible at ∼900, ∼680, 450−580, and below 400 cm^{-1}. The bands around 902 cm^{-1} and around 580 and 518 cm^{-1} were assigned to the symmetric stretching mode and the asymmetric modes of highly distorted TiO_6 octahedra, respectively. The additional band around 674 cm^{-1}, which is absent in the Raman spectra of $NaLnTiO_4$ with no central TiO_6 octahedra, was related to the slightly distorted central TiO_6 octahedra. The bands below 400 cm^{-1} were assigned to external modes located in the alkali-metal layer.

The Raman spectra of $A_2La_2Ti_3O_{10}$ (A = Na, K, and Rb) shown in Figure 3 could be explained by analogy with such assignments. Except for the band at 600−700 cm^{-1}, an overall shift of the Raman bands toward lower wavenumbers is observed in the region 400−1000 cm^{-1} on replacing Na by larger K and Rb, in agreement with an accompanied lattice expansion. In particular, the band at 902 cm^{-1} for $Na_2La_2Ti_3O_{10}$, which is assigned to the symmetric stretching mode of the short Ti(2)−O(4) bond (d = 1.702 Å) along the c axis, shifts to 875 and 867 cm^{-1} when Na is replaced by K and Rb, respectively. This remarkable Raman shift, which is consistent with a lengthening of Ti(2)−O(4) bond, appears to reflect an existence of linear A−O(4)−Ti(2) linkage as well as the lattice expansion. A variation of covalent character of the A−O(4) bond should strongly influence on the strength of competing Ti(2)−O(4) bond.

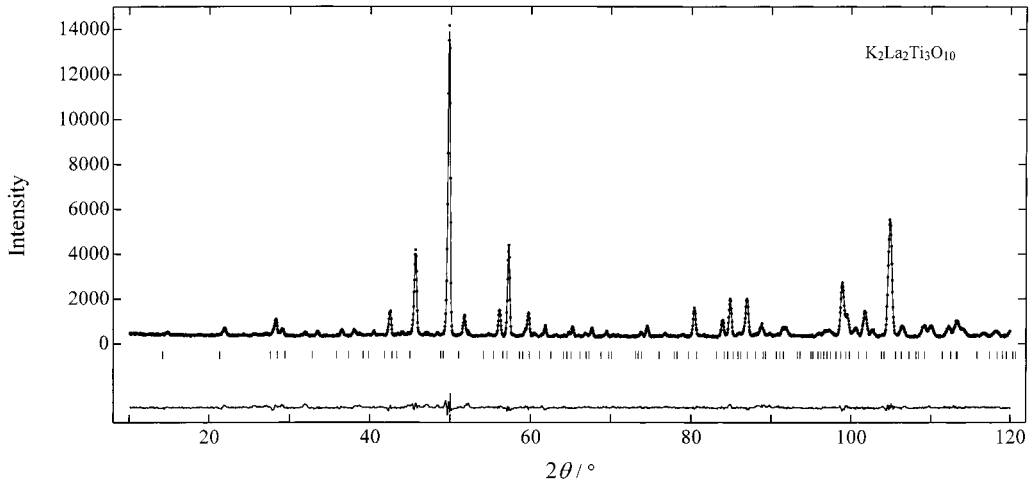

Figure 1. Calculated (solid line), experimental (dotted line), and difference (solid lines on the bottom) neutron powder diffraction pattern of $K_2La_2Ti_3O_{10}$.

Table 3. Refined Atomic Positions and Isotropic Temperature Factors of $A_2La_2Ti_3O_{10}$ (A = Na, K, and Rb)

compound	atom	position	g^a	x	y	z	B (Å^2)
$Na_2La_2Ti_3O_{10}$[b]	La	16n	4	0.020(5)	0.0	0.4255(1)	0.48(9)
	Na	16n	4	0.047(5)	0.0	0.2911(3)	0.65(25)
	Ti(1)	2a	2	0.0	0.0	0.0	-
	Ti(2)	4e	4	0.0	0.0	0.1496(2)	-
	O(1)	8j	4	0.111(1)	0.5	0.0	0.53(8)
	O(2)	16n	4	0.027(7)	0.0	0.0672(2)	1.07(20)
	O(3)	8g	8	0.0	0.5	0.1344(1)	0.70(4)
	O(4)	16n	4	0.028(7)	0.0	0.2090(2)	1.01(17)
$K_2La_2Ti_3O_{10}$	La	16n	4	0.01(4)	0.0	0.4280(1)	0.7(2)
	K	16n	4	0.0(5)	0.0	0.2923(3)	1.5(4)
	Ti(1)	2a	2	0.0	0.0	0.0	0.5(2)
	Ti(2)	4e	4	0.0	0.0	0.1411(2)	0.3(1)
	O(1)	8j	4	0.113(1)	0.5	0.0	0.7(1)
	O(2)	16n	4	0.019(9)	0.0	0.0640(2)	0.8(2)
	O(3)	8g	8	0.0	0.5	0.1281(1)	0.87(6)
	O(4)	16n	4	0.042(7)	0.0	0.1996(2)	0.6(3)
$Rb_2La_2Ti_3O_{10}$	La	16n	4	0.0(1)	0.0	0.4296(2)	0.6(2)
	Rb	16n	4	0.0(6)	0.0	0.2929(2)	1.6(3)
	Ti(1)	2a	2	0.0	0.0	0.0	0.9(2)
	Ti(2)	4e	4	0.0	0.0	0.1362(3)	0.2(2)
	O(1)	8j	4	0.106(1)	0.5	0.0	0.9(2)
	O(2)	16n	4	0.01(2)	0.0	0.0619(2)	1.1(3)
	O(3)	8g	8	0.0	0.5	0.1242(1)	0.93(8)
	O(4)	16n	4	0.035(9)	0.0	0.1941(2)	0.6(4)

[a] Unit cell occupancy. [b] Wright et al. (ref 26).

Table 4. Selected Bond Lengths (Å) and Bond Angles (deg) for $A_2La_2Ti_3O_{10}$ (A = Na, K, and Rb)

	$Na_2La_2Ti_3O_{10}$[a]	$K_2La_2Ti_3O_{10}$	$Rb_2La_2Ti_3O_{10}$
	Bond Length		
Ti(1)−O(1)	1.969(8)	1.996(1)	2.003(1)
Ti(1)−O(2)	1.924(7)	1.918(5)	1.900(7)
Ti(2)−O(2)	2.358(9)	2.310(8)	2.278(9)
Ti(2)−O(3)	1.971(8)	1.985(1)	1.993(2)
Ti(2)−O(4)	1.702(8)	1.762(8)	1.781(9)
	Bond Angle		
O(3)−Ti(2)−O(3)	154.5	157.4(3)	158.7(5)
Ti(1)−O(2)−Ti(2)	175	176(2)	177(5)

[a] Wright et al. (ref 26).

The bands around 540−590 cm^{-1} also shift to lower wavenumber. Its strong intensity suggests that this band is related to the highly distorted Ti(2)O_6 octahedra because it is forbidden for the regular octahedra. A splitting of the band by distortion is experimentally observed: 580 and 518 cm^{-1} for $Na_2La_2Ti_3O_{10}$, 558 and 513 cm^{-1} for $K_2La_2Ti_3O_{10}$, and 544 and 509 cm^{-1} for $Rb_2La_2Ti_3O_{10}$. But the extent of splitting decreases from

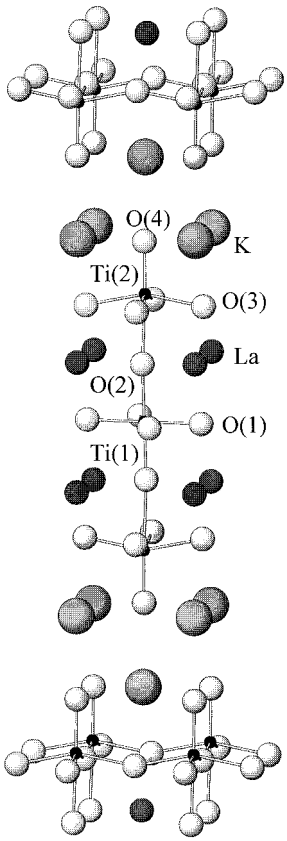

Figure 2. Idealized structure of $A_2La_2Ti_3O_{10}$. Only Ti−O bonds are described by lines. (Ti = black spheres, La = small shaded spheres, O = white spheres, and A = large shaded spheres.)

62 cm^{-1} to 45 and 35 cm^{-1}. Such a change points out that the symmetry of Ti(2)O_6 octahedra becomes more regular. This interpretation is well supported by the fact that the difference (Δ) between d{Ti(2)−O(2)} and d{Ti(2)−O(4)} decreases while the angle of O(3)−Ti(2)−O(3) bond increases in this sequence.

It should be noticed that the band at 600−700 cm^{-1}, in contrast to the other bands, shifts toward higher wavenumber from A = Na to K and Rb despite the lattice expansion. Interestingly, the shortening of the Ti(1)−O(2) bond shown in Table 4 coincides with the shifting tendency of this band. Its weak relative inten-

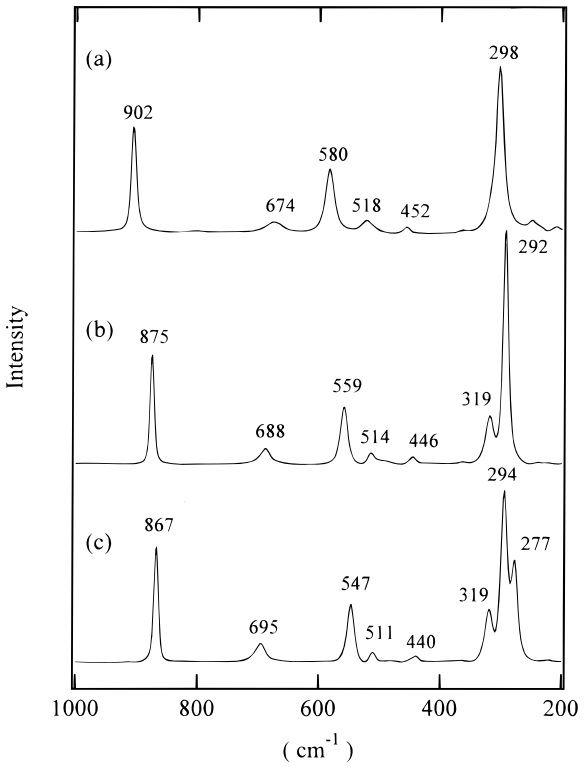

Figure 3. The Raman spectra of (a) $Na_2La_2Ti_3O_{10}$, (b) $K_2La_2Ti_3O_{10}$, and (c) $Rb_2La_2Ti_3O_{10}$.

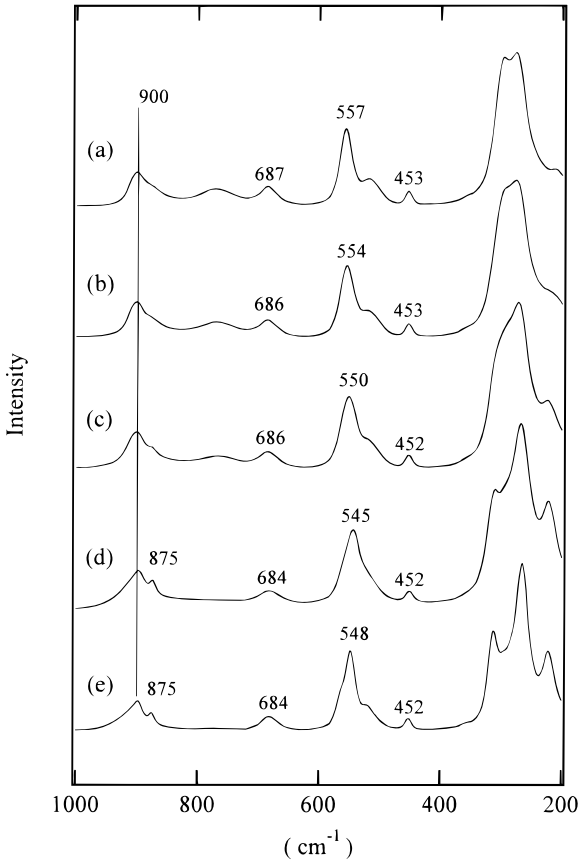

Figure 4. In-situ Raman spectra of $K_2La_2Ti_3O_{10}{\cdot}xH_2O$: hydrated state (a); heated at 80 °C (b), 120 °C (c), and 200 °C (d); and cooled to 30 °C (e).

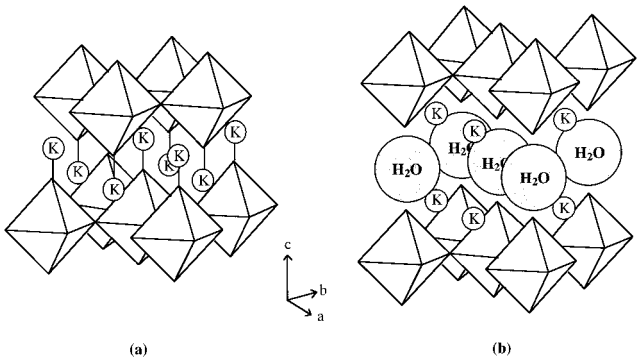

Figure 5. Idealized representations of the potassium ion layers of (a) $K_2La_2Ti_3O_{10}$ and (b) $K_2La_2Ti_3O_{10}{\cdot}2H_2O$. The insertion of water molecules into the potassium layers leads to a displacement of adjacent perovskite blocks toward eclipsed conformation. The bending of K−O−Ti linkage is induced by such a displacement. The TiO_6 unit is represented by an octahedron.

sity suggests again that this band should be related to the slightly distorted octahedra. Moreover, the change of bond length ratio (θ) of the axial Ti(1)−O(2) and equatorial Ti(1)−O(1) bonds, which decreases from 0.977 to 0.949, shows a parallel trend to an increase of the relative intensity of this band from A = Na to Rb. On the basis of such considerations, the band around 600−700 cm^{-1} must be attributed to the central $Ti(1)O_6$ octahedra whose symmetry is not strongly deviated from regular octahedra. This assignment agrees with the result of comparative study for the Raman spectra of $NaLnTiO_4$ and $Na_2Ln_2Ti_3O_{10}$.[22] In conclusion, the systematic Raman shifts shown in Figure 3 indicate that the structural variation of $A_2La_2Ti_3O_{10}$ (i.e., $m = 2$ members) is strongly dependent on the nature of alkali-metal atom.

The effect of water molecules, intercalated into the alkali-metal layers, on the local structure of layered titanates was investigated by in-situ Raman spectroscopy of $A_2La_2Ti_3O_{10}{\cdot}xH_2O$ (A = K and Rb, $x \approx 2$). As shown in Figure 4a, the Raman spectrum after hydration is quite different from that of unhydrated $K_2La_2Ti_3O_{10}$. The band at 875 cm^{-1} (whose relative intensity depends on the amount of intercalated water) strongly weakens, but instead new broad bands are observed at ~900 and ~770 cm^{-1} after hydration. The bands below 400 cm^{-1} are also strongly changed. The adjacent triple-octahedral layers have the staggered conformation in parent $K_2La_2Ti_3O_{10}$ as shown in Figure 5a. Because of the relative displacement of the potassium layer toward eclipsed conformation, however, the lattice *c* parameter is halved upon hydration.[5] This structural rearrangement is illustrated in Figure 5b. A significant change of the Raman bands below 400 cm^{-1} after hydration is consistent with such a rearrangement of the potassium layer. In this case, the resultant strong bending of K−O(4)−Ti(2) bonds will give the interlayer terminal O(4) atoms which can interact with the intercalated water molecules via hydrogen bonding. The band at ~900 cm^{-1} in Figure 4, which appears upon hydration, accordingly corresponds to the vibration of terminal Ti(2)−O(4) bond with double-bond character. Upon dehydration, the potassium layer would be rearranged to form again the linear K−O(4)−Ti(2) linkage as evidenced by an increase of the 875 cm^{-1} band intensity and the weakening of the 900 cm^{-1} band with increasing temperature. Unfortunately, a complete dehydration

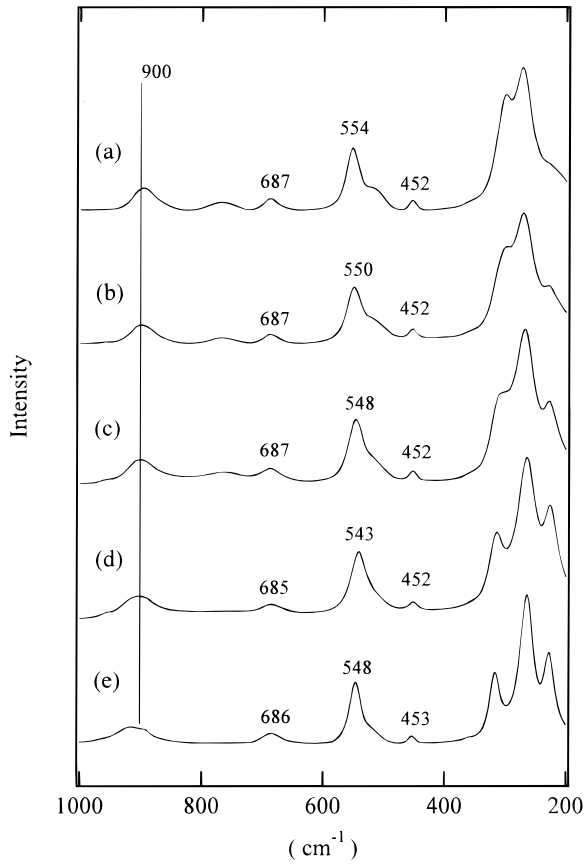

Figure 6. In-situ Raman spectra of $Rb_2La_2Ti_3O_{10}{\cdot}xH_2O$: hydrated state (a); heated at 80 °C (b), 120 °C (c), and 200 °C (d); and cooled to 30 °C (e).

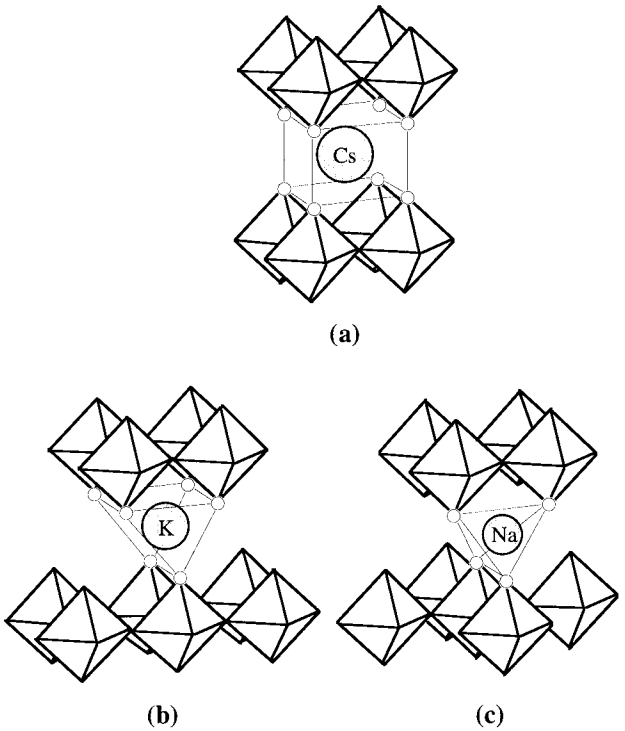

Figure 7. The possible coordination polyhedra for the A atoms of $A[Ca_2Nb_3O_{10}]$ or $A[LaNb_2O_7]$. Only the interlayer space is represented. The open circles are the O atoms and the octahedra represent NbO_6 unit.

was unsuccessful because our in-situ experiment was limited to 200 °C. (The temperature higher than 600 °C was required for the complete dehydration.) In-situ Raman spectra of $Rb_2La_2Ti_3O_{10}{\cdot}xH_2O$ are shown in Figure 6. What is the interesting aspect is that the Rb phase shows quite similar behaviors to the K analogue. In contrast to those of unhydrated forms, the Raman spectra of both hydrated ones show no significant Raman shift despite the change of alkali-metal layer (Figure 4a and 6a). All of these results propose that the alkali-metal layer of ion-exchangeable layered titanates strongly affects the local structure of TiO_6 octahedral layers only when there is a linear A−O−Ti connection. This picture could be confirmed by the Raman spectra of ion-exchangeable layered niobates with no such linear linkages.

Raman Spectra of $ACa_2Nb_3O_{10}$ and $ALaNb_2O_7$ (A = Na, K, Rb, and Cs) and $CsB_2Nb_3O_{10}$ (B = Ca, Sr, and Ba). Overall structural features of the triple-octahedral slab for $m = 1$, $n = 3$ members are similar to those for $m = 2$, $n = 3$ ones. Thus, the perovskite slabs of $ACa_2Nb_3O_{10}$ (A = alkali metal) are composed of highly distorted outer NbO_6 octahedral layers and slightly distorted central NbO_6 one.[3,4,8] However, the interlayer A atoms occupy several kinds of coordination sites between the octahedral layers depending on their sizes. As illustrated in Figure 7a, the eclipsed conformation of adjacent octahedral layers gives a distorted cubic site which is filled with a large A atom such as Cs. If the adjacent perovskite slabs are relatively displaced by $a/2$ each other, a trigonal prismatic site is then induced (Figure 7b). This site is occupied by a medium-size A atom such as K. On the other hand, a tetrahedral site resulting from a displacement of adjacent layers toward complete staggered conformation are filled with a small A cation such as Na and Li (Figures 7c). A formation of trigonal prismatic or tetrahedral site in the interlayer space is accompanied by a c axis doubling. Concerning $m = 1$, $n = 2$ members such as $ALaM_2O_7$ (A = alkali metal and M = Nb or Ta), no central octahedra is contained in their structures because they are composed of strongly distorted double-octahedral layers only. But their alkali-metal layers retain the same structural characteristics with those of $m = 1$, $n = 3$ members.[7,9,18,27,29] Therefore, it was expected that the bands related to the central NbO_6 octahedra can be easily assigned by comparing the Raman spectra of these two series. In addition, it should be noted that the structures of $m = 1$ and 2 members have an important difference from each other in bonding nature of the alkali-metal atom. While there is always a linear A−O−Ti linkage parallel to the c axis in $m = 2$ members, no structure for $m = 1$ members has a linear A−O−Nb connection. Such a structural feature suggests that the nature of A atom will not greatly affect the Nb−O bond vibration along the c axis.

Figures 8 and 9 show the Raman spectra of $ACa_2Nb_3O_{10}$ and $ALaNb_2O_7$ (A = Na, K, Rb, and Cs), respectively. The assignment of the Raman bands for $KCa_2Nb_3O_{10}$ has been carried out by Jehng et al.[30] They

(27) Sato, M.; Abo, J.; Jin, T.; Ohta, M. *Solid State Ionics* **1992**, *51*, 85.
(28) Kumada, N.; Kinomura, N.; Sleight, A. W. *Acta Crystallogr. C* **1996**, *52*, 1063.
(29) Toda, K.; Uematsu, K.; Sato, M. *J. Ceram. Soc. Jpn.* **1997**, *105*, 482.

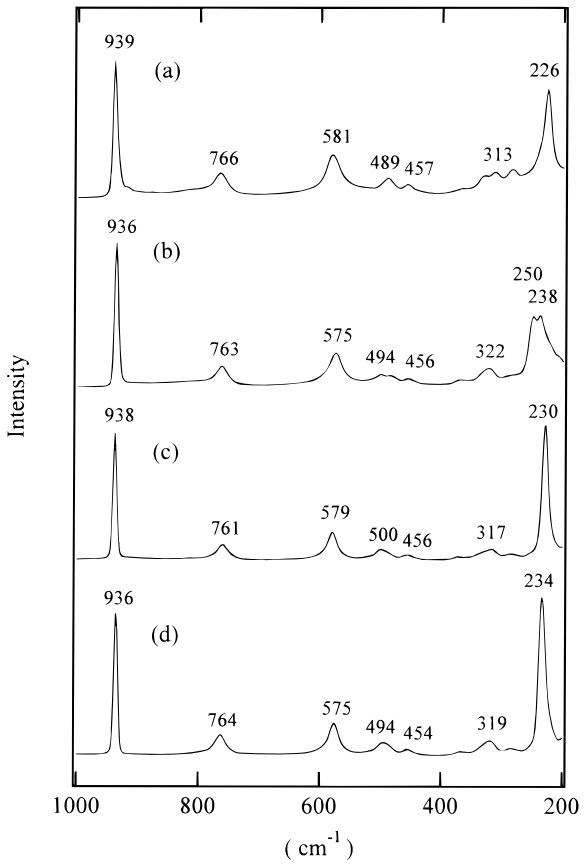

Figure 8. The Raman spectra of (a) $NaCa_2Nb_3O_{10}$, (b) $KCa_2Nb_3O_{10}$, (c) $RbCa_2Nb_3O_{10}$, and (d) $CsCa_2Nb_3O_{10}$.

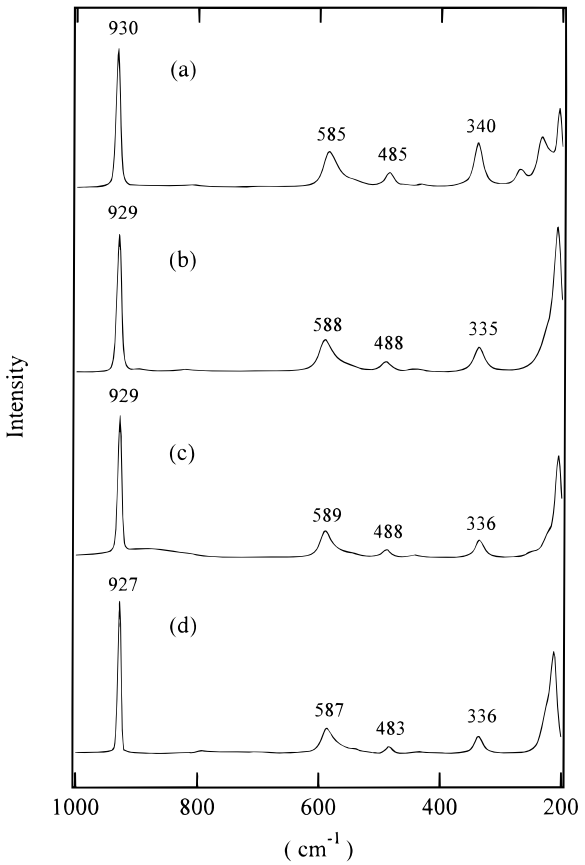

Figure 9. The Raman spectra of (a) $NaLaNb_2O_7$, (b) $KLaNb_2O_7$, (c) $RbLaNb_2O_7$, and (d) $CsLaNb_2O_7$.

interpreted the band around 930 cm^{-1} to be associated with the highly distorted NbO_6 octahedra. Comparison of the intensity ratio of the band at 760 and 580 cm^{-1} of $KCa_2Na_{n-3}Nb_nO_{3n+1}$ ($n = 3-5$) led to assign these bands to the slightly distorted central NbO_6 site modes.

According to such assignments, a sharp strong band around 930 cm^{-1} in Figure 8 would be assigned to the vibrational mode of the Nb−O terminal bond of highly distorted NbO_6 octahedra. On the contrary, a different interpretation could be given for the band at ∼580 cm^{-1}. If we compare the Raman spectra of $ACa_2Nb_3O_{10}$ and $ALaNb_2O_7$, the bands around 930 cm^{-1} is common to all these oxides. The bands around 580 and 480 cm^{-1} are also observed in both spectra. Comparing the structure of octahedral layers, these common bands should be attributed to the highly distorted NbO_6 octahedra because they are contained in both types of oxide. In contrast to $ACa_2Nb_3O_{10}$, however, $ALaNb_2O_7$ shows no Raman band at 600−800 cm^{-1}. Consequently, an additional band around 760 cm^{-1} in Figure 8 must be due to the slightly distorted central NbO_6 octahedra.

Of the most interest to us is that all the Raman bands in the region 400−1000 cm^{-1} of Figures 8 and 9 are essentially constant regardless of the identity of alkali-metal layers. These results are in contrast to the Raman spectra of unhydrated $A_2La_2Ti_3O_{10}$ ($m = 2$ members) which shows a strong dependence on the alkali-metal layer. Instead, such a constant Raman behavior is quite similar to that of hydrated forms $A_2La_2Ti_3O_{10}{\cdot}xH_2O$ with no A−O−Ti linkage. Accordingly, the absence of linear A−O−Nb connection would be responsible for the completely contrast Raman shifts of $ACa_2Nb_3O_{10}$ and $ALaNb_2O_7$ to that of $A_2La_2Ti_3O_{10}$ with linear A−O−Ti

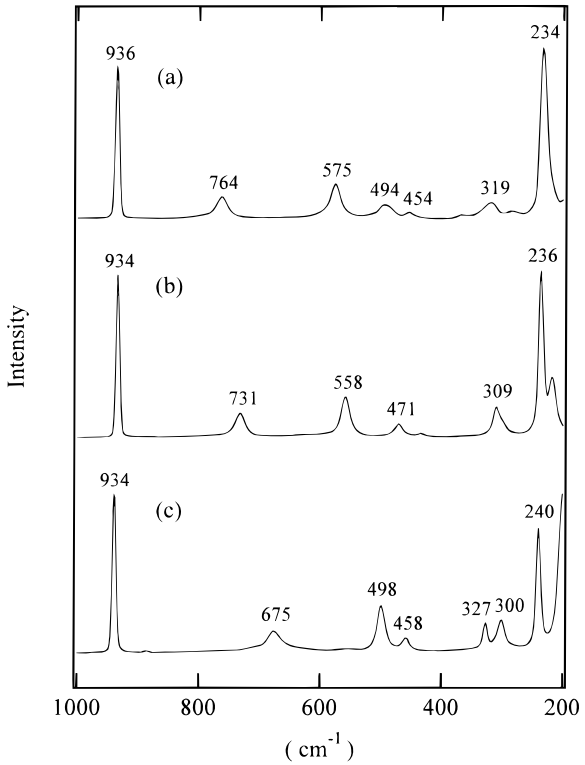

Figure 10. The Raman spectra of (a) $CsCa_2Nb_3O_{10}$, (b) $CsSr_2Nb_3O_{10}$, and (c) $CsBa_2Nb_3O_{10}$.

(30) Jehng, J.-M.; Wachs, I. E. *Chem. Mater.* **1991**, *3*, 100.

bond. The more extreme example is given in the Raman spectra of $CsB_2Nb_3O_{10}$ (B = Ca, Sr, and Ba) shown in Figure 10. In this series, a replacement of the B atom from Ca to Sr and Ba, which occupy 12-coordinate sites as found in the perovskite lattice, is accompanied by a large expansion of triple-octahedral slab. A remarkable shift of the bands around 760, 570, and 490 cm^{-1} toward lower wavenumber is in agreement with such an expansion. Nevertheless the band around 930 cm^{-1} is not displaced at all. No shift of this band indicates that the terminal Nb−O bond with double-bond character is affected neither by the expansion of the perovskite layer nor by the change of interlayer space.

Conclusions

Neutron diffraction study showed that the A−O−Ti bond is practically linear in the structure of $A_2La_2Ti_3O_{10}$ (A = Na, K, and Rb). Because of such a linear linkage, the nature of interlayer A atom strongly influences on the distortion of TiO_6 octahedra. Comparison of the Raman spectra and structural data of ion-exchangeable layered perovskites indicated that the most important factor to determine their Raman shifts is the bonding mode between the interlayer alkali-metal atoms and multiple-octahedral layers. One of the interesting aspects is that the local structure of perovskite slab is essentially independent of the alkali-metal layer if there is no linear linkage between each layer. An existence or absence of the linear linkage between them can be also confirmed by the characteristic band around 850−930 cm^{-1}. From understanding such Raman spectroscopic features, the change of interlayer space during interlayer reaction could be explained without knowledge of the exact crystal structure. Therefore, the interlayer structure−Raman spectra relationship developed here should serve in rationally designing the catalysts for specific purposes and in understanding the interlayer chemistry of ion-exchangeable layered perovskites.

Acknowledgment. We are grateful to the MOST for providing the program to use of Neutron diffraction facilities at the KAERI. H.-J.N. thanks the Ministry of Education for the studentship through BK21 program. This work was supported by grant 981-0308-046-2 from the Basic Research program of the KOSEF.

CM9906506